Journal of Materials Processing Technology 216 (2015) 48–58

Contents lists available at ScienceDirect

Journal of Materials Processing Technology

journal homepage: www.elsevier.com/locate/jmatprotec

Characterization of the deformation field in large-strain extrusion machining

S.L. Cai, Y. Chen, G.G. Ye, M.Q. Jiang, H.Y. Wang, L.H. Dai*

State Key Laboratory of Nonlinear Mechanics, Institute of Mechanics, Chinese Academy of Sciences, No. 15 North Fourth Ring Road Weat, Beijing 100190, China

ARTICLE INFO

Article history:
Received 1 April 2014
Received in revised form 20 July 2014
Accepted 23 August 2014
Available online 6 September 2014

Keywords:
Extrusion machining
Shear strain
Severe plastic deformation

ABSTRACT

Large-strain extrusion machining (LSEM) has been emerged as a promising severe plastic deformation methodology for the creation of nano or ultra-fined grained materials. To realize deformation control, the key issue involved is the strain estimation in LSEM. In order to characterize the deformation field in LSEM, the experiments of LSEM oxygen-free high-conductivity copper were conducted by using a specially designed LSEM device. Based upon the deformation field measured by high speed imaging and digital image correlation (DIC), a new strain estimation model considering the extrusion process of constraint is proposed in this paper. The theoretical predicted strain agrees well with the measurements.

1. Introduction

Metal cutting, simply machining, is a process of removal of excess material from the workpiece in the form of chips. Over the past decades, Oxley (1989) and Shaw (2005) have been carried out a series of work to discover the fundamental mechanisms underlying the metal machining processes. According to the extensive study of Childs (2013), machining has been proved to be a particularly effective method to achieve severe plastic deformation (SPD). Compared to the conventional SPD methods such as equal channel angular pressing (Segal et al., 1981), high pressure torsion (Smirnova et al., 1986) and surface mechanical attrition treatment (SMAT) (Tao et al., 2002), the SPD method of machining needs only one single pass of deformation process to produce large strains in removed chips and high strength materials are much easier to be deformed in this manner. Materials undergoing SPD often result in the variation of microstructure within the materials in the work of Mueller and Mueller (2007). Recently, Güzel et al. (2012) researched dynamic grain structure evolution of materials in SPD and found that grain size decreases with increasing equivalent plastic strain. According to the study of Lu et al. (2004), the materials with SPD have enhanced mechanical properties with raising both the strength and the thermal stability. Yan et al. (2012) further found that strength and ductility are both increased by means of SPD with high strain rates. As for the SPD of machining, Brown et al. (2002) first used the low-cost method to produce nanostructured materials. Shankar et al. (2005) and Swaminathan et al. (2005) then applied the machining method to study microstructure refinement as a function of deformation condition for different metals. Deng et al. (2009) further developed a realistic finite element model to research the relationship between the formation of ultra-fine grained materials by machining and large shear strain imposed in deformation fields. In the previous studies, a relatively low cutting speed is applied to avoid the thermal effect on the produced microstructure during machining. Recently, even with very high cutting speed, Kanani et al. (2014) found that it is possible to produce continuous chip with a stable nano-and ultra-fine grained structure by choosing a proper machining condition. Therefore, machining is a promising SPD method to produce materials with enhanced mechanical properties by controlling the level of SPD in machining.

The level of strain in SPD machining is constant if the machining parameters (rake angle and precut chip thickness) are given in advance. In order to control the level of deformation in machining, De Chiffre (1976) first puts forward the extrusion-machining process and made use of the process to produce materials of different mechanical properties by changing the controlled chip thickness ratio. After three decades, Moscoso et al. (2007) perform seminal works where large-strain extrusion machining (LSEM) is developed to create nano or ultra-fined grained materials. LSEM is an improved technique of SPD machining. Compared with the conventional SPD machining, LSEM can control the level of

* Corresponding author. Tel.: +86 10 82543958; fax: +86 10 82543977.
E-mail address: lhdai@lnm.imech.ac.cn (L.H. Dai).

http://dx.doi.org/10.1016/j.jmatprotec.2014.08.022
0924-0136/

deformation even if the rake angle and precut chip thickness are given in advance. Saldana et al. (2010) further find that the chips' microstructures and properties are tightly related to the controlling plastic deformation in LSEM. The experiments of Moscoso et al. (2007) and Saldana et al. (2010) have shown that LSEM can be applied to a variety of metals (e.g., copper, titanium, Al6061-T6) for producing UFG microstructures. Particularly for copper, an elongated UFG microstructure is obtained at the shear strain level of 2.2 in LSEM, and a mix of elongated and equi-axed UFG microstructure can be seen in materials at the shear strain level of 4.3 in LSEM, and the essentially equi-axed UFG structures with nano-size grains (~250 nm) can be produced if the level of shear strain in LSEM is above 7.4. Brown et al. (2009) observe the increase in the proportion of high angle boundary misorientation with increasing strain at small deformation rates, which results in the grain refinement in LSEM. The microstructure in UFG materials is directly related to the level of strain in LSEM. Therefore, in order to control the microstructure in UFG materials much better, it is crucial to determine the plastic strain during LSEM in advance. Based on the single shear-plane model, De Chiffre (1976) derived an expression of shear strain in primary shear zone in chips in LSEM, where the constraint effect during extrusion machining was neglected. However, the recent measurements of the deformation field in LSEM made by Guo et al. (2012) and Efe et al. (2012) using high speed imaging and particle image velocimetry (PIV) have demonstrated that the difference between the PIV measured strain and the Chiffre's model predicted strain becomes more prominent with decreasing the chip thickness ratio. Hence, to obtain reasonable strain estimation in LSEM, the effect of the chip thickness ratio or the geometrical constraint should be incorporated.

In this paper, in order to investigate the effect of the geometrical constraint on the strain field during LSEM, a commercial grade oxygen-free high-conductivity (OFHC) copper (99.95%) was machined at different levels of strain by using a specially designed LSEM device. By making use of high speed imaging and digital image correlation (DIC), the detailed features of the material particle flow field in chip in LSEM were measured. Based on the experimental observation, an explicit expression of shear strain in LSEM is presented in the paper where the extrusion constraint effect during machining process is included. The predicted strains are consistent well with the present experimental results and the other available measurements.

2. Experimental procedure

The sample materials used in the experiments is oxygen-free high-conductivity (OFHC) copper (99.95%) with chemical composition specified in Table 1. The annealing temperature of OFHC is 375–650 °C. The samples were taken from OFHC copper bar and the microstructures of three section planes in the workpiece are shown in Fig. 1.

Fig. 1 shows the device of LSEM which is conducted on material testing machine. The chip thickness t_c is controlled by the constraint in LSEM. Fig. 2 shows a schematic of LSEM, in which the free machining (FM) is marked by the dashed lines. Here, an orthogonal machining process is taken into consideration, where a wedge-shaped tool with a rake angle α is static, and the workpiece with a precut depth t_0 is moving toward the tool at the cutting speed V. According to the books of Oxley (1989) and Shaw (2005), it is assumed that the pure plastic deformation happens in machining. Based on the tensile tests of OFHC copper in Appendix A, the elastic strain is less than 0.5% but the plastic strain in LSEM is more than 100%. It is reasonable to ignore the occurrence of elastic strain and subsequent recovery in LSEM. Here, the elastic deformation is ignored and the pure plastic deformation is assumed in LSEM. In this process, the workpiece materials in the cutting layer flow out along the rake face of the tool in the form of a chip with a thickness t_c. The levels of large plastic strain in LSEM are controlled by the chip thickness ratio ($\lambda = t_c/t_0$). The chip is formed by a process of shear which is approximately confined to a single plane called shear plane OA. The inclined angle φ of shear plane is named as

Table 1
Chemical composition of oxygen-free high-conductivity copper (99.95%).

Elements	Cu + Ag	Fe	S	Pb	Zn	Sn	O	Others
Wt.(%)	99.97	0.004	0.004	0.003	0.003	0.002	0.002	0.01

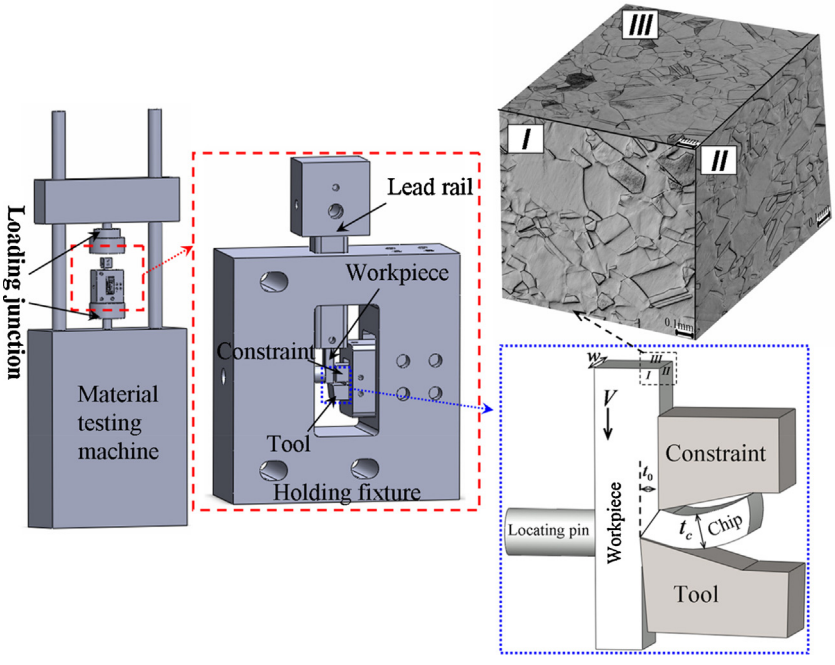

Fig. 1. Schematic of LSEM processes and the microstructures of three section planes I, II and III of workpiece.

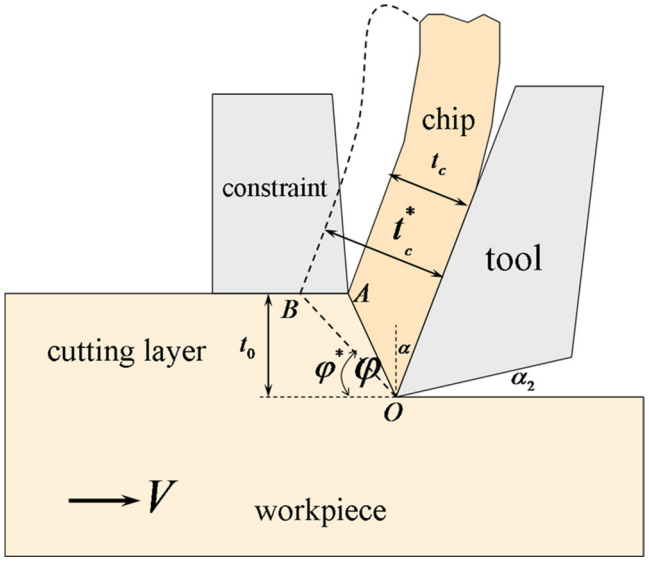

Fig. 2. Schematic for plane-strain LSEM processes with parameters, and the dashed lines denote the FM case.

Table 2
Cutting condition in FM.

Cutting parameters	Notation	Value
Rake angle	α	10°
Clearance angle	α_2	5°
Precut chip thickness	t_0	100, 150, 200, 250 μm
Cutting width	w	5 mm
Cutting speed	V	10 μm/s
Chip thickness	t_c	FM

shear angle. In the FM case, we assume that the shear plane is along OB with the shear angle φ^*, and the thickness of chip formed is t_c^*.

Commercial grade, OFHC copper was machined at different constraint levels by using the LSEM set-up in Fig. 1. First, in order to obtain the chip thickness ratio for FM ($\lambda^* = t_c^*/t_0$), the experiments of FM OFHC were conducted under the following conditions listed in Table 2. Then, OFHC copper was machined at different levels of SPD during LSEM under the conditions of Table 3. Dewes et al. (1999) found that high cutting speed results in high strain rates, elevating temperatures in materials. According to the research of De Chiffre (1983), the rise of temperature consequently anneals the ultra-fine grain (UFG) materials produced in LSEM. In order to avoid the annealing of UFG materials, low cutting speed is required in LSEM. By using the infrared thermography, Huang et al. (2008) has confirmed that the relatively low cutting speed was selected to ensure minimal temperature rise in PSZ. In the experiments of Kashfuddoja et al. (2014) and Wang et al. (2014), the techniques such as high speed imaging and digital image correlation (DIC) have been proved to be reliable for the analysis of strain field. According to the calibration results in Fig. A2 of Appendix A, the maximum deviation between DIC and extensometer is less than 5 percent, and therefore, the techniques such as high speed imaging and DIC are credible to be used in LSEM. During the machining, a high-speed camera (Photron SA-X2-480K-M1, maximum frame rate $3.24 \times 10^4\ s^{-1}$), positioned stationary with respect to PSZ, was used to image the deformation zone (see in Videos 1 to 6 in Appendix B). A 1 × 1 mm region of the machining zone was imaged at 50 fps at a spatial resolution of ~1 μm per pixel. Digital image correlation (DIC), a powerful available optical-numerical method capable of measuring full-field displacement without contact (VIC -2D Image Correlation Software, Correlated Solutions, Inc.), was used to directly map the strain fields in PSZ. After machining, chips were collected and embedded into clean resin. The lateral process was mechanically polished and then the polished surfaces were etched in a 120 ml·H_2O + 50 ml HCl + 10 g $FeCl_3$ solution lasting for 15 s to reveal the deformed microstructure. These etched specimens were observed with the optical microscope (Olympus BX51 M) to examine the morphologies of chips.

Table 3
Cutting condition in LSEM.

Cutting parameters	Notation	Value
Rake angle	α	10°
Clearance angle	α_2	5°
Precut chip thickness	t_0	200 μm
Cutting width	w	5 mm
Cutting speed	V	10 μm/s
Controlled chip thickness	t_c	FM, 600, 500, 400, 300, 200 μm
Controlled chip thickness ratio	λ_c	λ^*, 3.0, 2.5, 2.0, 1.5, 1.0
Measured chip thickness ratio	λ	3.55, 2.76, 2.35, 1.81, 1.38, 0.87

3. Experimental observations

Fig. 3 shows the experimental results in FM for different precut chip thicknesses t_0, and then the chip thickness ratio λ^* in FM could be measured in Fig. 3. The measured chip thickness ratios for different precut chip thicknesses are illustrated in Fig. 4. According to Fig. 4, the chip thickness ratios λ^* in FM are almost equal to 3.5. Therefore, the chip thickness ratio λ^* in FM is assumed to be 3.5 in this paper.

Fig. 5 shows the microstructures of chips at different constraint levels (λ = 0.87 to 3.55 (FM)). Compared with the microstructure of samples in Fig. 1, the microstructure of materials does not evolve until the materials move into PSZ. As shown in Fig. 6, it is implied that the strain fields before PSZ are different from that behind PSZ. By making use of high speed imaging and DIC, the strain fields at different constraint levels are illustrated in Fig. 7 (λ = 0.87 to 3.55 (FM)). As seen in Fig. 7, the small level of SPD is imposed on the materials before moving into PSZ, but the materials have experienced large level of SPD during moving out of PSZ.

According to the strain fields, the variation of equivalent plastic strain with along pathline abcd (Fig. 6) is achieved at different constraint levels. Fig. 8 shows the measurements of equivalent plastic strain with along pathline abcd. Because the flow in LSEM is steady state, these pathlines are also streamlines whose tangents represent velocity directions. Based on the relationship between equivalent plastic strain and time at different constraint levels (λ = 0.87 to 3.55 (FM)), the equivalent plastic strain rises sharply in PSZ and achieves a relative stable value after moving out of PSZ.

By making further use of DIC, the detailed features of the material particle flow field in chips during LSEM were measured. The existence of the constraint makes the materials moving into the shear plane not along the original direction any longer, but having a deviating angle β (see in Fig. 6). Fig. 9 shows the streamlines during LSEM experiments at different constrain levels (λ = 0.87 to 3.55 (FM)), and the inclined angle β between streamlines and cutting speed direction (OB) is measured before moving into PSZ (OA). From the streamlines at different constraint levels, the constraint does exert a significant influence on the machining process. The inclined angle β increases with the decreasing chip thickness ratio, which means that the constraint has an effect on the direction of materials moving into PSZ during LSEM. The materials moving into PSZ is not along the original direction of cutting speed any longer, but has a deviating angle β.

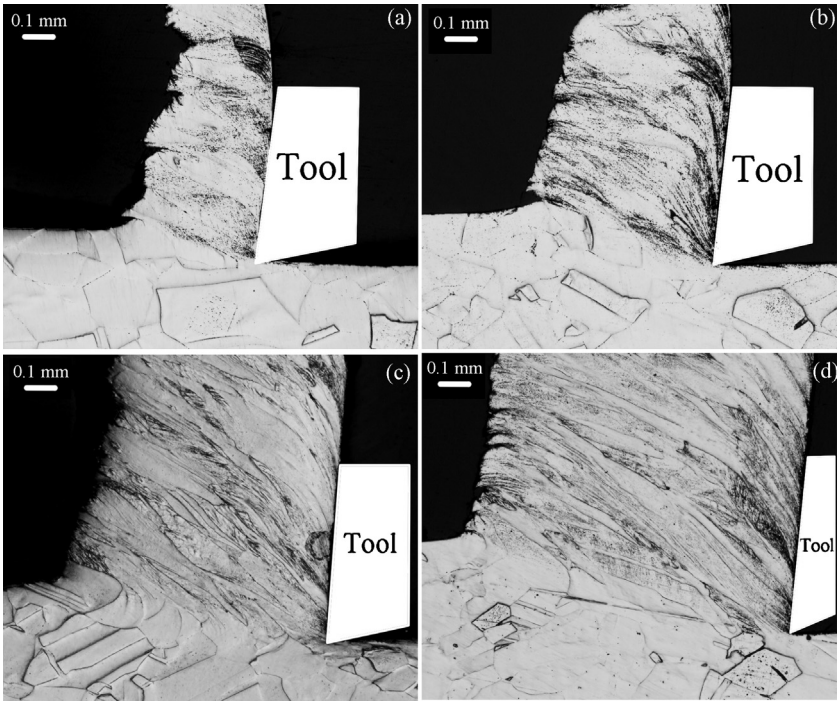

Fig. 3. The experimental results in FM for different precut chip thicknesses t_0: (a) t_0 = 100 μm; (b) t_0 = 150 μm; (c) t_0 = 200 μm; (d) t_0 = 250 μm.

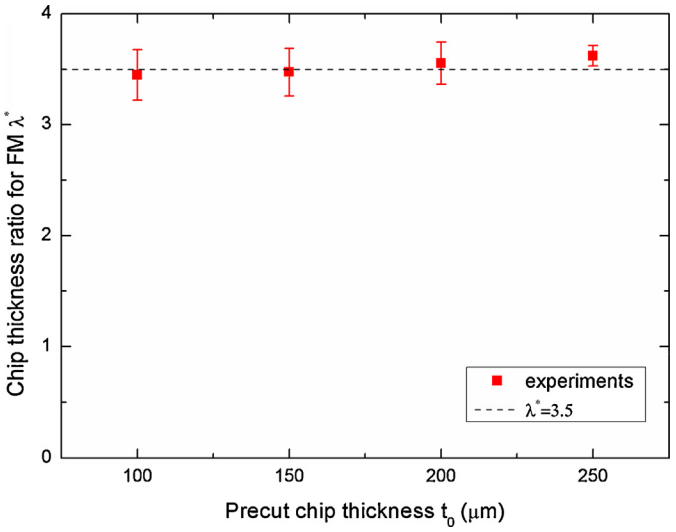

Fig. 4. The measured chip thickness ratios for different precut chip thicknesses.

4. Theoretical model

The symbols used in the paper are listed in Table 4 before the theoretical derivation. For FM, the constraint has no influence on the machining process and the deviating angle β is nearly zero (see in Fig. 9). Merchant (1945) derived the shear strain along the shear plane:

$$\gamma^* = \frac{\cos\alpha}{\sin\varphi^* \cos(\varphi^* - \alpha)} \tag{1}$$

where the shear angle φ^* of FM can be obtained from the chip thickness ratio $\lambda^* = t_c^*/t_0$ as:

$$\tan\varphi^* = \frac{\cos\alpha}{\lambda^* - \sin\alpha}. \tag{2}$$

Table 4
Symbols used in the paper.

Parameters	Notation
Rake angle	α
Precut chip thickness	t_0
Chip thickness in FM	t_c^*
Chip thickness ratio in FM	$\lambda^* \left(\lambda^* = t_c^*/t_0\right)$
Controlled chip thickness in LSEM	$t_c\,(t_c \le t_c^*)$
Chip thickness ratio in LSEM	$\lambda \left(\lambda = t_c/t_0 \le \lambda^*\right)$
Shear angle in FM	φ^*
Shear angle in LSEM	$\varphi\,(\varphi \ge \varphi^*)$
Deviating angle	β
Shear strain in Chiffre's model	γ^*
Shear strain in present model	γ

For the FM, λ^* is actually a material-dependent parameter, and the range of λ^* is 1–15 for various metallic materials. However, the chip thickness ratio can be adjusted by changing the geometrical constraint level, in order to obtain different level of shear strain. This is the essentials of the LSEM as shown in Fig. 2. In the LSEM case with the geometrical constraint, the thickness of chip formed changes into t_c with the chip thickness ratio $\lambda = t_c/t_0$ and the corresponding shear plane changes into the OA with the shear angle φ. Chiffre directly used the expression of shear strain in FM to estimate the shear strain in LSEM where the extrusion effect was completely ignored, and then the shear strain in LSEM is given by De Chiffre (1976):

$$\gamma^* = \frac{\lambda}{\cos(\alpha)} + \frac{1}{\lambda\cos(\alpha)} - 2\tan(\alpha). \tag{3}$$

It is noted that Eq. (3) is the same as the shear strain formula in FM and the effect of constraint is ignored. However, the most prominent difference between LSEM and FM is the introduction of constraint in LSEM. Hence, the influence of constraint should be taken into consideration to obtain reasonable strain field estimation in LSEM. It can be seen from Fig. 9 that the constraint has a significant influence on the flow field in LSEM. In fact, the existence of the constraint makes the materials moving into the shear plane

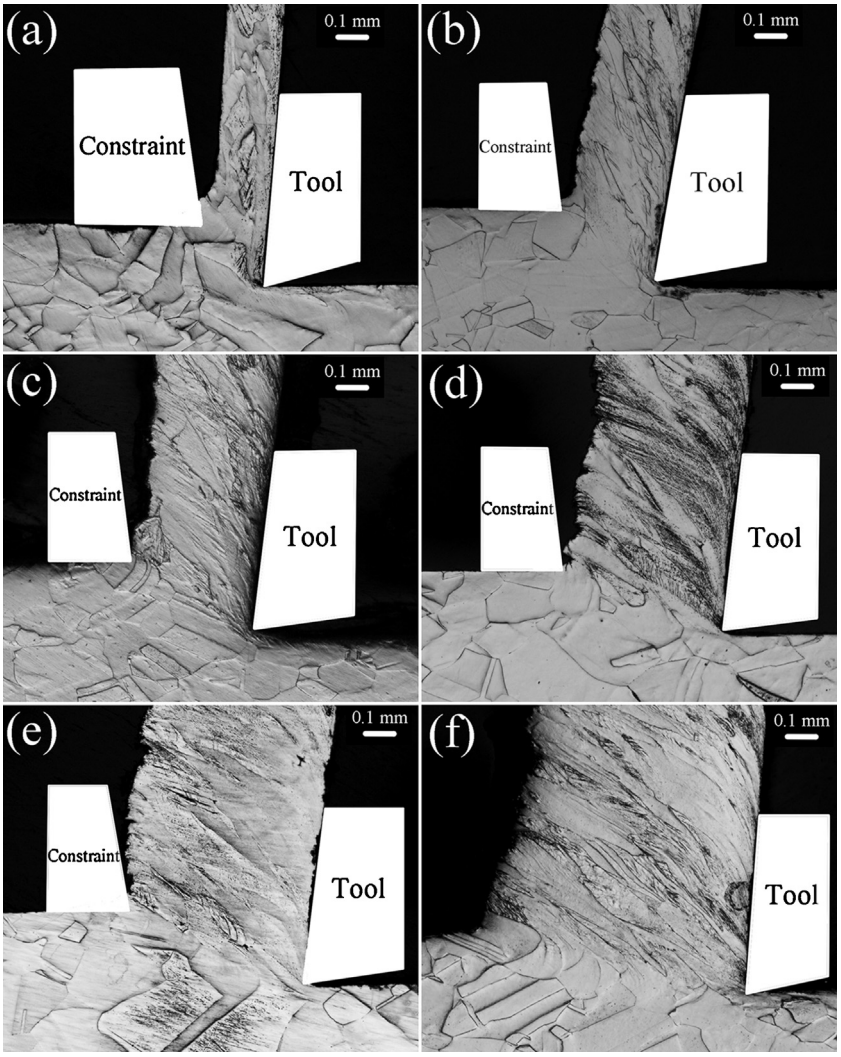

Fig. 5. Microstructures of chips at different constraint levels: (a) λ = 0.87; (b) λ = 1.38; (c) λ = 1.81; (d) λ = 2.35; (e) λ = 2.76; (f) FM.

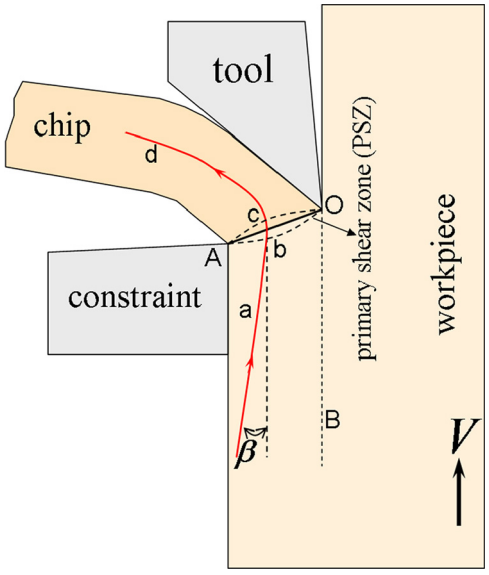

Fig. 6. Schematic of material flow undergoing LSEM and red line abcd represents pathline.

not along the original direction any longer, but having a deviating angle β. Such a material flow process has been clearly observed in the LSEM experiments of OFHC, and so does in recent LSEM experiments conducted by Guo et al. (2012). The LSEM process is very similar to that in a nonequal channel angle pressing process put forward by Hasani et al. (2010). As shown in Fig. 10a, when the materials move to shear plane OA along the channel *A′AO′O*, the materials should be sheared immediately by the tool and flow out along the rake face of the tool in the form of a chip. During such a process, the shear strain imposed in the materials can be calculated as:

$$\gamma = \frac{\Delta S}{\Delta d}, \tag{4}$$

where $\Delta S = \Delta d \times \cot\left(\varphi - \beta\right) + \Delta d \times \cot\left(\left(\pi/2\right) - \varphi + \alpha\right)$. Thus the shear strain (4) changes into:

$$\gamma = \frac{1 + \tan\varphi \tan\beta}{\tan\varphi - \tan\beta} + \tan\left(\varphi - \alpha\right) \tag{5}$$

In this expression, shear angle φ is determined by $\tan\varphi = \cos\alpha/(\lambda - \sin\alpha)$ and the deviating angle β is unknown.

As shown in Fig. 10b, the constraint extrudes the excessive materials (e.g. triangle *ABC* in the FM) into the workpiece along the shear plane OA. It is reasonable to envision that the intruded materials by the constraint entirely move into the region of

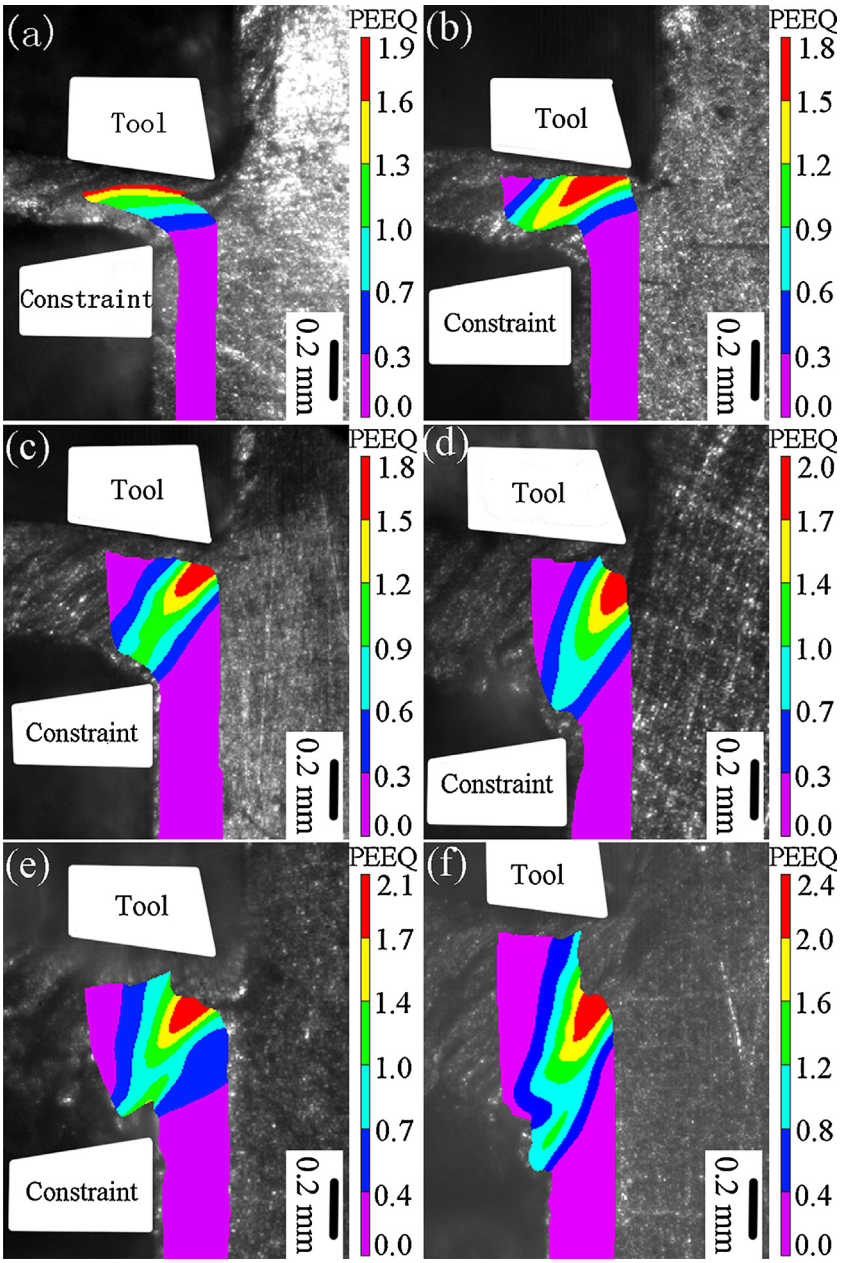

Fig. 7. Equivalent plastic strain fields at different constraint levels: (a) $\lambda = 0.87$; (b) $\lambda = 1.38$; (c) $\lambda = 1.81$; (d) $\lambda = 2.35$; (e) $\lambda = 2.76$; (f) FM.

triangle *ODE*. Then $\angle ODE = \beta$ is obtained. Obviously, according to the trigonometric relation:

$$\tan\beta = \frac{EF}{OD + EF\cot\varphi} \tag{6}$$

where $OD = t_0\cot\varphi^*$ and *EF* is pending. In particular, the area of triangle *ABC* is equal to that of triangle *ODE* because of incompressible materials, so *EF* is obtained as:

$$EF = t_0\left(\frac{\lambda^*}{\lambda - 1}\right)\left(1 - \frac{\cot\varphi}{\cot\varphi^*}\right). \tag{7}$$

Combining Eqs. (6) and (7), the deviating angle β is given out:

$$\tan\beta = \frac{(\lambda^* - \lambda)^2\cos\alpha}{\lambda(\lambda^* - \sin\alpha)^2 + (\lambda - \sin\alpha)(\lambda^* - \lambda)^2}. \tag{8}$$

Then substituting Eq. (8) into Eq. (5), the shear strain formula characterizing the deformation in LSEM is obtained as:

$$\gamma = \frac{\lambda - \sin\alpha + \cos\alpha\tan\beta}{\cos\alpha - (\lambda - \sin\alpha)\tan\beta} + \frac{1}{\lambda\cos\alpha} - \tan\alpha \tag{9}$$

where $\tan\beta$ is given by Eq. (8).

It is noted that the shear strain formula given by Eq. (9) is related to not only the machining parameters (e.g. rake angle α and chip thickness ratio λ) but also the material property λ^* in β. It is expected that, when λ approaches to λ^*, that is, $\lambda/\lambda^* \to 1$, the LSEM is actually the FM. It is must be pointed out that the new model can totally capture this trend.

5. Comparison of model and experimental results

To demonstrate the rationality of the assumption in the new model, the machining parameters in the experiments are substituted into the deviating angle (8) to compare with the experimental

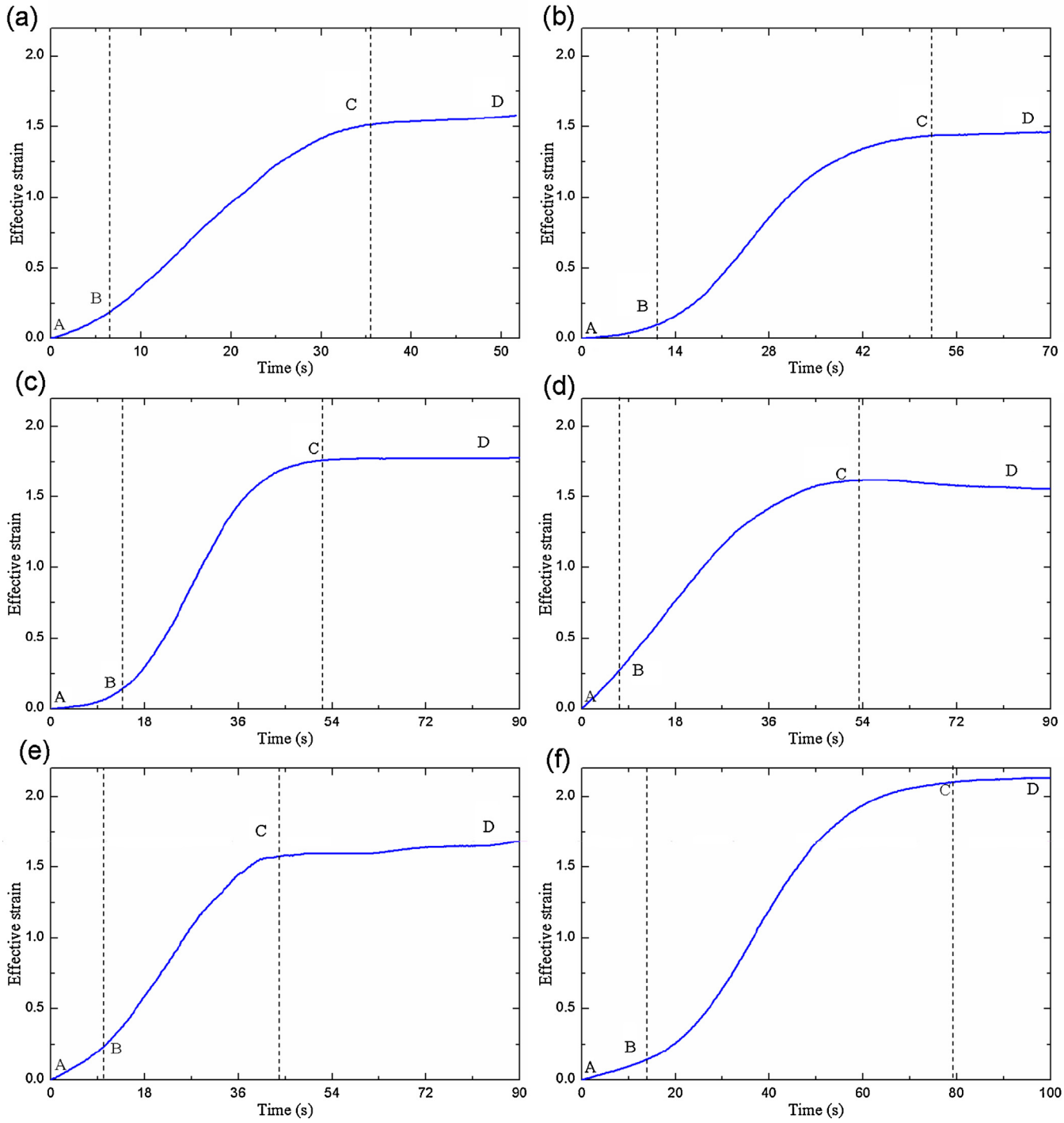

Fig. 8. Equivalent plastic strain along pathline ABCD at different constraint levels: (a) λ = 0.87; (b) λ = 1.38; (c) λ = 1.81; (d) λ = 2.35; (e) λ = 2.76; (f) FM.

and theoretical values. As shown in Fig. 11, the theoretical predictions are almost identical with the experimental values. It is also reasonable, especially for FM where the deviating angle β becomes zero, which accords with the available experimental results of Gnanamanickam et al. (2009). According to the above discussions, it is logical to assume that the materials moving into PSZ has a deviating angle in LSEM.

In order to further validate the model proposed in the present study, the new model is used to predict the experimental results and the available experimental results of Guo et al. (2012). As shown in Fig. 12a, the present model exhibits a very good prediction of the present experimental results when the machining and property parameters in our own LSEM experiments are substituted into the proposed model (9), where the effective strain $\bar{\varepsilon}$ can be obtained by the shear strain γ as $\bar{\varepsilon} = \gamma/\sqrt{3}$. Recently, Guo et al. (2012) and Efe et al. (2012) performed an elegant work for measuring the deformation field in LSEM by using high-speed imaging and PIV method. By carrying out a discrete summation of the incremental shear strains along a particle trajectory, the total shear strain imposed in the material over its entire history of deformation can be obtained. When the machining and property parameters in the experiments of Guo et al. (2012) are substituted into the proposed model (9), the new model exhibits a very good prediction of the experimental results (see in Fig. 12b). For comparison, the

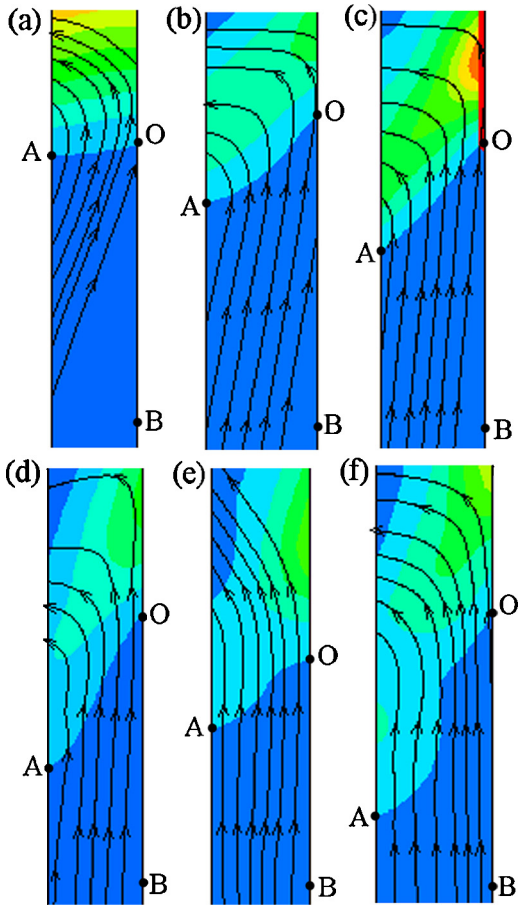

Fig. 9. Streamlines of flow field in the cutting layer at different levels: (a) λ = 0.87; (b) λ = 1.38; (c) λ = 1.81; (d) λ = 2.35; (e) λ = 2.76; (f) FM.

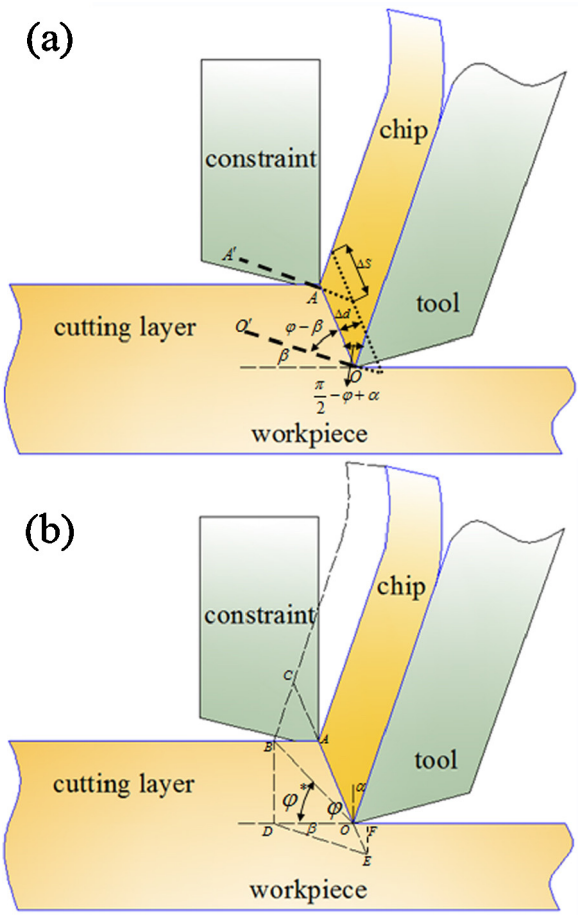

Fig. 10. (a) Channel of materials flowing denoted by the dashed lines in LESM. (b) Extrusion process from constraint in LSEM.

predicted result of the Chiffre's model (3) is also shown in Fig. 12 as a dash line. It can be seen that the trends predicted by both models are similar to that seen in the experimental measurements. However, the measured strains are greater than those estimated by the model of Chiffre, with the extent of deviation increasing with the decrease of chip thickness ratio. Especially for the small thickness chip ratio, the extrusion effect of the constraint is notable and large differences appear if the extrusion of constraint is ignored in the model of De Chiffre (1976). The extrusion of constraint is taken into consideration and the materials property is introduced into the present shear strain formula, i.e., Eq. (9), so the strains calculated are more accurate. The new theoretically prediction is much close to the experimental measured results.

6. Discussions

The main reason of the deviation between the targeted chip thickness ratio and the achieved chip thickness ratio is the machining tolerance of the proposed experimental set-up. In order to confirm that the present LSEM experimental set-up is valid to control deformation field in machining, the comparison between the targeted level of strain and the achieved level of strain is listed in Table 5. According to the comparison in Table 5, the maximum deviation between the targeted chip thickness ratio and the achieved chip thickness ratio is about 13 percent because of the machining tolerance of experimental set-up, but the maximum deviation between the targeted level of strain and the achieved level of strain is less than 6 percent. Although the proposed experimental set-up

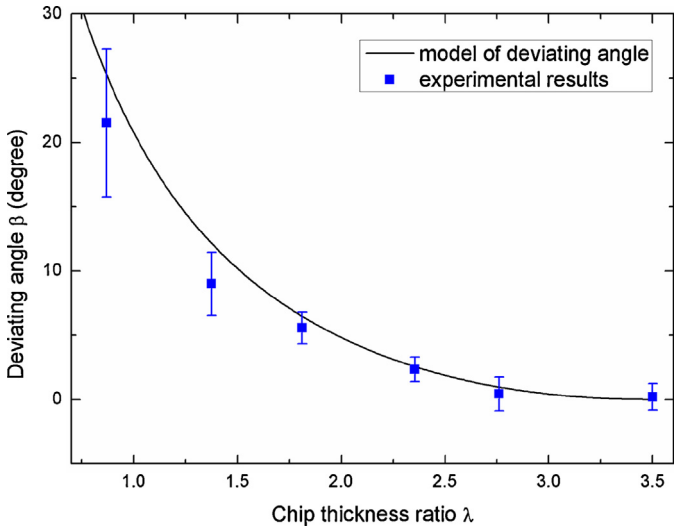

Fig. 11. Variation of deviating angle β with chip thickness ratio λ and compared with the experimental measurements.

is not much accurate to control the chip thickness ratio, it is valid to control the deformation field in LSEM.

Compared with the model of De Chiffre (1976), the shear strain formula (9) is more reasonable to characterize the deformation field in LSEM. The model of De Chiffre (1976) is directly borrowed from strain estimation of FM model by replacing λ^* in FM by λ. Such a treatment results in an obvious illegitimacy. When different

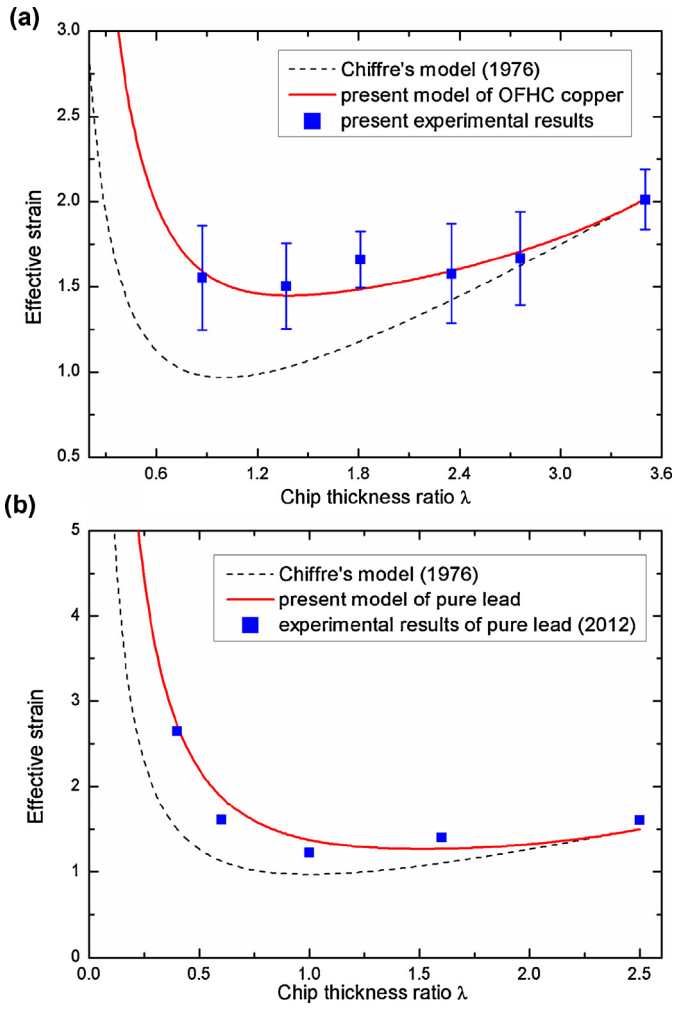

Fig. 12. Variation of the effective strain with chip thickness ratio estimated by the new model proposed in the paper and model of De Chiffre (1976): (a) Compared with the present experimental results; (b) In comparison with the experimental results of Guo et al. (2012).

Table 5
Comparison between the targeted level of strain and the achieved level of strain.

Parameters	Value					
Targeted chip thickness ratio	3.5	3.0	2.5	2.0	1.5	1.0
Achieved chip thickness ratio	3.55	2.76	2.35	1.81	1.38	0.87
Relative deviation	1.4%	8.0%	6.0%	9.5%	8.0%	13%
Targeted level of strain	2.01	1.79	1.63	1.52	1.45	1.51
Achieved level of strain	2.02	1.70	1.59	1.49	1.44	1.59
Relative deviation	0.4%	5.0%	2.4%	2.0%	0.7%	5.3%

workpiece materials (with different λ^*) are machined by using the identical machining parameters (with identical λ) in LSEM, Chiffre's model always gives the identical shear strains. But the new model (9) can predict different shear strains for different materials. In fact, the parameter λ^* denotes the level that the chip can expand freely in FM, while λ is a machining parameter that can be controlled in advance by adjusting the position of the constraint in the LSEM. Usually, λ is set to be smaller than λ^* in order to obtain different levels of strain in LSEM. As shown in Fig. 13a, for different λ^*, if $\lambda/\lambda^* \to 1$, the deviating angle β becomes zero. Under this condition, the new model (9) is totally the same as the Chiffre's model (3). Under the condition where the material property λ^* varies and the machining parameters are identical, the relationships between the two shear strain models and chip thickness ratio λ are drawn in

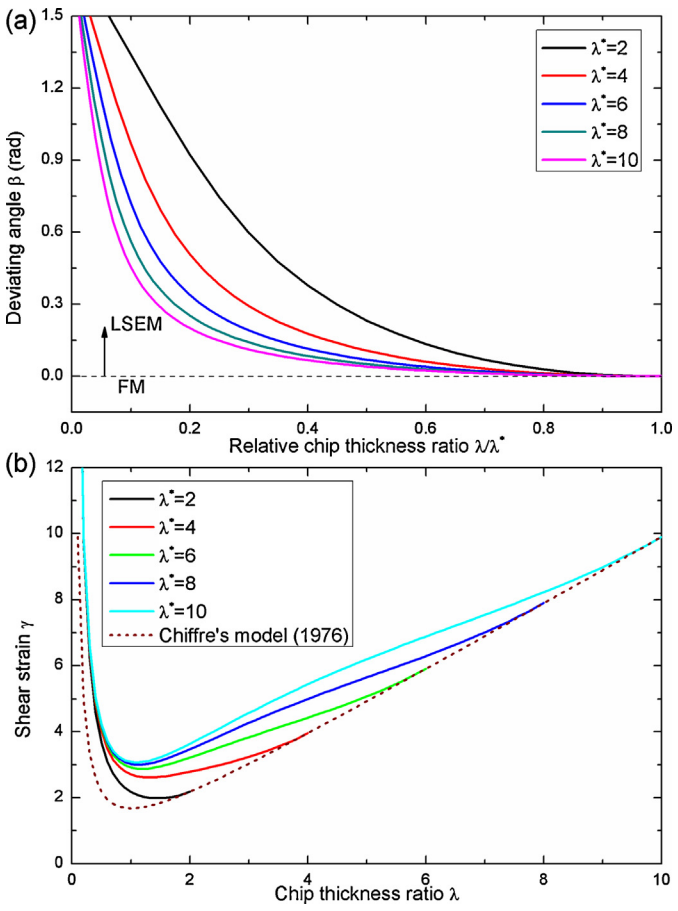

Fig. 13. (a) Variation of deviating angle β with chip thickness ratio λ normalized by λ^*. (b) Variation of shear strain γ with λ when different materials are machined in LSEM.

Fig. 13b. It is noted that, for different materials (with different λ^*), the new model gives different strain values for a given λ. However, the Chiffre's model seems to give the low bound of strains and does not distinguish the strain in LSEM different materials.

7. Summary and conclusions

In summary, the geometrical constraint is found to have a significant influence on the deformation field in LSEM. According to the observation of flow field in the experiments of LSEM, the constraint changes the velocity direction of the materials moving into PSZ. Based on the detailed observation, a new shear strain model to estimate the shear strain in the deformation field in LSEM is proposed in this paper where the extrusion process of constraint is taken into consideration. The new shear strain formula is related to not only the machining parameters but also the material parameters. Compared with the conventional model of Chiffre, the shear strains calculated by the new model are more accurate allowing for the effect of extrusion from the constraint. The shear strains predicted by the new model are much better consistent with the experimental results than those of the conventional model. The new shear strain formula proposed in the paper is very useful for using LSEM to create nano or ultra-fined grained materials.

Acknowledgements

The work is supported by the National Natural Science Foundation of China (Grant Nos. 11132011, 11402278, 11372315 and

11202221), the National Basic Research Program of China (Grant No. 2012CB937500) and the CAS/SAFEA International Partnership Program for Creative Research Teams.

Appendix A.

The tensile tests of oxygen-free high-conductivity (OFHC) copper were conducted at the loading rate of 1 mm/min, and the strain of digital image correlation (DIC) was compared with that of extensometer. Fig. A1 shows the specimen size and the relationship of stress and strain in tensile tests. The tensile zone was imaged at 50 fps during tensile tests, and then DIC was used to directly measure the strain in tensile tests. The strain comparisons between DIC and extensometer in tensile tests are shown in Fig. A2. As seen in Fig. A2, the tendencies of strain between DIC and extensometer are the same, and the maximum deviation between them is less than 5 percent. The comparison results prove that the high speed imaging and DIC techniques are reliable to analyze the deformation field.

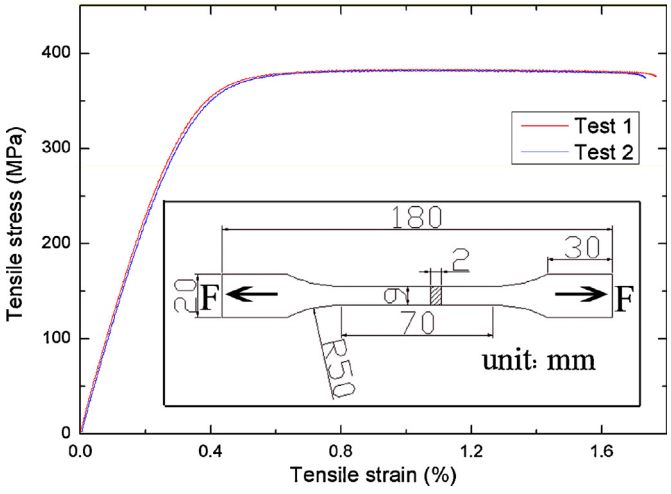

Fig. A1. The specimen size and the relationship of stress and strain in tensile tests.

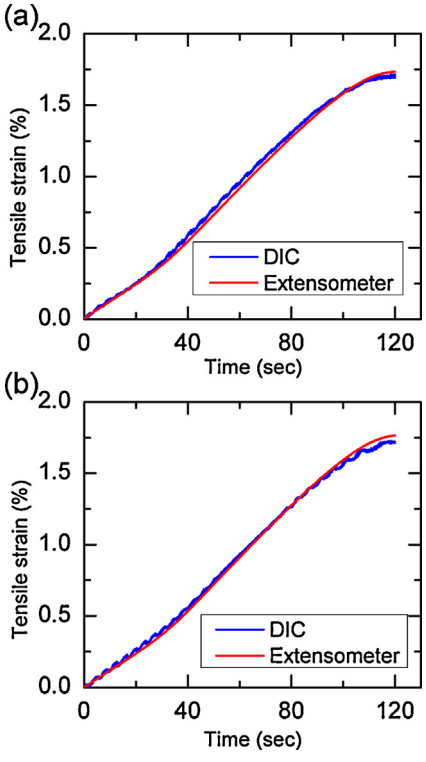

Fig. A2. The strain comparisons between DIC and extensometer in tensile tests: (a) the comparisons in test 1; (b) the comparisons in test 2.

Appendix B.

Supplementary data associated with this article can be found, in the online version, at http://dx.doi.org/10.1016/j.jmatprotec.2014.08.022.

References

Brown, T.L., Swaminathan, S., Chandrasekar, S., Compton, W.D., King, A.H., Trumble, K.P., 2002. Low-cost manufacturing process for nanostructured metals and alloys. J. Mater. Res. 17, 2484–2488.
Brown, T.L., Saldana, C., Murthy, T.G., Mann, J.B., Guo, Y., Allard, L.F., King, A.H., Compton, W.D., Trumble, K.P., Chandrasekar, S., 2009. A study of the interactive effects of strain, strain rate and temperature in LSEM of copper. Acta Mater. 57, 5491–5500.
Childs, T.H.C., 2013. Ductile shear failure damage modelling and predicting built-up edge in steel machining. J. Mater. Process. Technol. 213, 1954–1969.
De Chiffre, L., 1976. Extrusion-cutting. Int. J. Mach. Tool Des. Res. 16, 137–144.
De Chiffre, L., 1983. Extrusion cutting of brass strips. Int. J. Mach. Tool Des. Res. 23, 141–151.
Deng, W.J., Xia, W., Li, C., Tang, Y., 2009. Formation of ultra-fine grained materials by machining and the characteristics of the deformation fields. J. Mater. Process. Technol. 209, 4521–4526.
Dewes, R.C., Ng, E., Chua, K.S., Newton, P.G., Aspinwall, D.K., 1999. Temperature measurement when high speed machining hardened mould/die steel. J. Mater. Process. Technol. 92–93, 293–301.
Efe, M., Moscoso, W., Trumble, K.P., Dale Compton, W., Chandrasekar, S., 2012. Mechanics of LSEM and application to deformation processing of magnesium alloys. Acta Mater. 60, 2031–2042.
Gnanamanickam, E.P., Lee, S., Sullivan, J.P., Chandrasekar, S., 2009. Direct measurement of large-strain deformation fields by particle tracking. Meas. Sci. Technol. 20 (9), 095710.
Guo, Y., Efe, M., Moscoso, W., Sagapuram, D., Trumble, K.P., Chandrasekar, S., 2012. Deformation field in LSEM and implications for deformation processing. Scr. Mater. 66, 235–238.
Güzel, A., Jäger, A., Parvizian, F., Lambers, H.G., Tekkaya, A.E., Svendsen, B., Maier, H.J., 2012. A new method for determining dynamic grain structure evolution during hot aluminum extrusion. J. Mater. Process. Technol. 212, 323–330.
Hasani, A., Toth, L.S., Beausir, B., 2010. Principles of nonequal channel angular pressing. J. Eng. Mater. Technol.-Trans. ASME 132 (3), 031001.
Huang, C., Murthy, T.G., Shankar, M.R., M'Saoubi, R., Chandrasekar, S., 2008. Temperature rise in severe plastic deformation of titanium at small strain-rates. Scr. Mater. 58, 663–666.
Kanani, M., Sohrabi, S., Ebrahimi, R., Paydar, M.H., 2014. Continuous and ultra-fine grained chip production with large strain machining. J. Mater. Process. Technol. 214, 1777–1786.
Kashfuddoja, M., Prasath, R.G.R., Ramji, M., 2014. Study on experimental characterization of carbon fiber reinforced polymer panel using digital image correlation: a sensitivity analysis. Opt. Lasers Eng. 62, 17–30.
Lu, L., Shen, Y.F., Chen, X.H., Qian, L.H., Lu, K., 2004. Ultrahigh strength and high electrical conductivity in copper. Science 16, 422–426.
Merchant, M.E., 1945. Mechanics of the metal cutting process. I. Orthogonal cutting and a type 2 chip. J. Appl. Phys. 16, 267–275.
Moscoso, W., Shankar, M.R., Mann, J.B., Compton, W., Chandrasekar, S., 2007. Bulk nanostructure materials by LSEM. J. Mater. Res. 22, 201–205.
Mueller, K., Mueller, S., 2007. Severe plastic deformation of the magnesium alloy AZ31. J. Mater. Process. Technol. 187–188, 775–779.
Oxley, P.L.B., 1989. Mechanics of Machining: An Analytical Approach to Assessing Machinability. Wiley, New York, NY.
Saldana, C., Swaminathan, S., Brown, T.L., Moscoso, W., Mann, J.B., Compton, W.D., Chandrasekar, S., 2010. Unusual applications of machining: controlled nanostructuring of materials and surfaces. J. Manuf. Sci. Eng.-Trans. ASME 132 (3), 030908.
Segal, V.M., Reznikov, V.I., Drobyshevskiy, A.E., Kopylov, V.I., 1981. Plastic working of metals by simple shear. Russ. Metall. 1, 99–105.
Shankar, M.R., Chandrasekar, S., King, A.H., Compton, W.D., 2005. Microstructure and stability of nanocrystalline aluminum 6061 created by large strain machining. Acta Mater. 53, 4781–4793.
Shaw, M.C., 2005. Metal Cutting Principles, second ed. Oxford University Press, Oxford.
Smirnova, N.A., Levit, V.I., Pilyugin, V.I., Kuznetsov, R.I., Davydova, L.S., Sazonova, V.A., 1986. Evolution of the fcc single-crystal structure during severe plastic deformations. Fiz. Met. Metalloved. 61, 1170–1177.

Swaminathan, S., Shankar, M.R., Lee, S., Hwang, J., King, A.H., Kezar, R.F., Rao, B.C., Brown, T.L., Chandrasekar, S., Compton, W.D., Trumble, K.P., 2005. Large strain deformation and ultra-fine grained materials by machining. Mater. Sci. Eng., A 410–411, 358–363.

Tao, N.R., Wang, Z.B., Tong, W.P., Sui, M.L., Lu, J., Lu, K., 2002. An investigation of surface nanocrystallization mechanism in Fe induced by surface mechanical attrition treatment. Acta Mater. 50, 4603–4616.

Wang, K., Carsley, J.E., He, B., Li, J., Zhang, L., 2014. Measuring forming limit strains with digital image correlation analysis. J. Mater. Process. Technol. 214, 1120–1130.

Yan, F.K., Liu, G.Z., Tao, N.R., Lu, K., 2012. Strength and ductility of 316L austenitic stainless steel strengthened by nano-scale twin bundles. Acta Mater. 60, 1059–1071.